

Robotic Pick-and-Place Operations in Multifunctional Liquid Crystal Elastomers

Pengrong Lyu, Mert Orhan Astam, Carlos Sánchez-Somolinos, and Danqing Liu*

Pick-and-place operations for transporting objects precisely to a target position are a prominent function of (soft-) robotic systems. Therefore, there is great interest in industry to improve the characteristic gripping, holding, and releasing methods involved in pick-and-place operations. Within living organisms such as octopi, nature demonstrates that multiple types of conjointly working actuators are required for flexible pick-and-place operations. Herein, a multifunctional soft robotic arm is developed, capable of transporting an object within 3D space. The soft robotic arm consists of two structural actuators (rotating base and lifting unit) and a suction cup-based gripper. The structural actuator acts as both the load bearing and actuating components of the robotic system. Yet, the gripper is the crucial innovation within the robotic arm. A cephalopod-limb-inspired gripper functioning through the reversible flat-to-conical deformation of azimuthally aligned liquid crystal elastomer (LCE) films is proposed. The pressure-generating actuation mechanism of the gripper means that no external device is needed to operate the gripping function. Akin to natural systems, the in-tandem operation of the actuators in the soft robotic arm allows for multifactored tasks. Yet, the design achieves this through the use of a single material, which is not innate in natural archetypes.

tailored for delicate applications, such as surgery or prosthetics.^[2] Within these robotic applications, pick-and-place operations to precisely transport objects are common and essential functions. Typical robotic arm designs are inspired by the human arm, consisting of a hard metal frame with multiple protruding “fingers” and joints.^[3–5] Recently, soft materials, such as silicone, have been applied in robotic arms to enhance their adaptability to various environments.^[6–8] Typically, these systems are operated with controlled air pressure and are easy to fabricate^[9–11] but require external valves, tubes, and bulky motors. Meanwhile, robotic motions such as contracting,^[12,13] bending,^[14–16] and rolling^[17] functions have been demonstrated by stimuli-responsive materials. However, unlike natural systems, state-of-the-art stimuli-responsive material actuators are typically designed for a single function, which renders them unable to perform multifactored tasks.


Therefore, in this work, we developed and designed a soft robotic arm capable of multifactored pick-and-place operations, incorporating the function of the stimuli-responsive material rotating base, lifting unit, and suction cup-based gripper (Figure 1a). The soft robotic arm can operate within 3D space, without the need for integration with any external motor. Each actuator in the soft robotic arm can be individually controlled via electrical signals, enabling

1. Introduction

(Micro-) robots are globally ubiquitous.^[1] Capable of working under extreme, human-adverse conditions, robots have extended the potential of industry to unprecedented heights. Robots can be used to perform heavy or repetitive tasks, such as shifting components between production lines. Yet, robots can also be

P. Lyu, M. O. Astam, D. Liu
Institute for Complex Molecular Systems
Eindhoven University of Technology
Den Dolech 2, 5612 AZ Eindhoven, The Netherlands
E-mail: d.liu1@tue.nl

P. Lyu, M. O. Astam, D. Liu
Department of Chemical Engineering and Chemistry
Eindhoven University of Technology
Den Dolech 2, 5612 AZ Eindhoven, The Netherlands

 The ORCID identification number(s) for the author(s) of this article can be found under <https://doi.org/10.1002/aisy.202200280>.

© 2022 The Authors. Advanced Intelligent Systems published by Wiley-VCH GmbH. This is an open access article under the terms of the Creative Commons Attribution License, which permits use, distribution and reproduction in any medium, provided the original work is properly cited.

DOI: 10.1002/aisy.202200280

C. Sánchez-Somolinos
Instituto de Nanociencia y Materiales de Aragón (INMA)
Departamento de Física de la Materia Condensada
CSIC-Universidad de Zaragoza
Zaragoza 50009, Spain

C. Sánchez-Somolinos
CIBER in Bioengineering, Biomaterials and Nanomedicine (CIBER-BBN)
Spain

D. Liu
SCNU-TUE Joint Lab of Device Integrated Responsive Materials (DIRM)
National Center for International Research on Green Optoelectronics
South China Normal University
Guangzhou Higher Education Mega Center, No 378, West Waihuan Road,
510006 Guangzhou, China

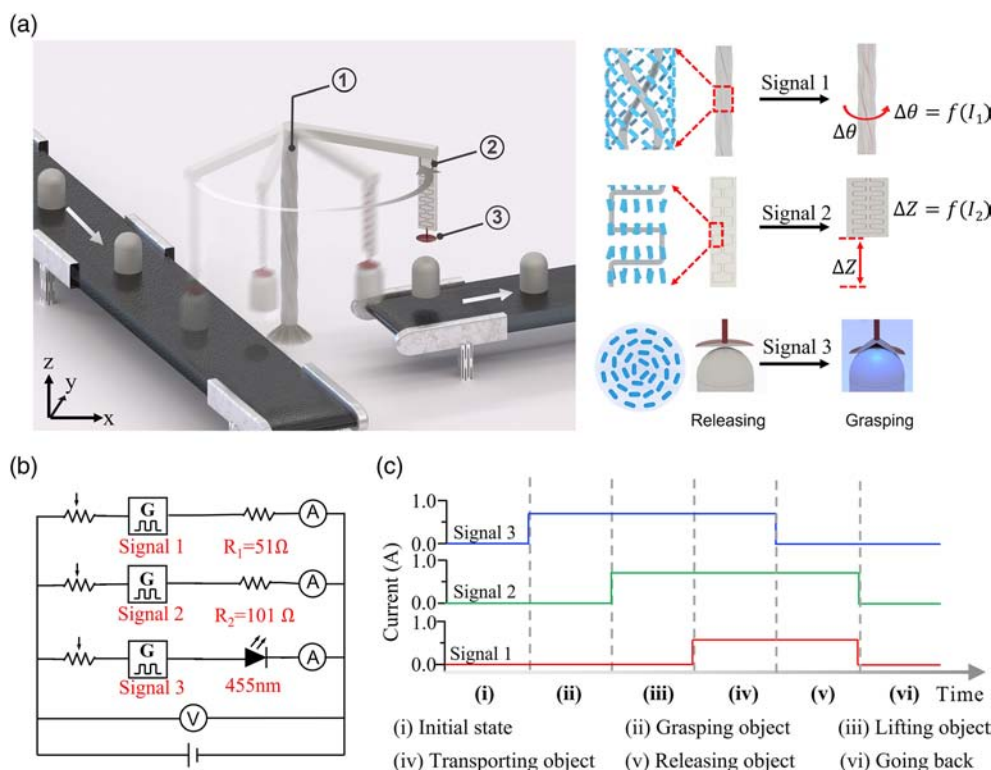


Figure 1. Principle of the multifunctional soft robotic arm. a) The schematic of the soft robotic arm and its components. b) Equivalent electrical circuit of the electrical-driving set-up within the soft robotic arm. R_1 and R_2 correspond to the resistance of the nichrome heating wire embedded in the rotating base and lifting unit respectively. c) The driving electric signal inputs for controlling the different elements of the soft robotic arm: signal 1 for actuating the rotating base, signal 2 for actuating the lifting unit, and signal 3 for actuating the gripper.

the capacity to program its movement and operate it repetitively. The actuation behavior of each component is pre-designed by controlling molecular alignment architecture, which is a fundamental concept in the field of liquid crystals.

Liquid crystal elastomers (LCEs) consist of polymerized liquid crystals, networked by bonds to chain-extending molecules. These materials have gained recognition as stimuli-responsive actuators, leading to their application in artificial muscles,^[18–22] artificial walkers,^[15,23,24] responsive topography,^[25,26] etc. Inspired by prior art, we constructed a photothermal-responsive LCE suction cup. Upon deformation of the azimuthally aligned (Figure 1a) LCE from its flat to conical state, negative pressure is generated, adhering the target object to the LCE cup. Meanwhile, to transport the object in 3D space, a rotating base with helical alignment is responsible for the motion in X- and Y-axes. On the other hand, motion in the Z-axis is achieved through an additional lifting unit with uniaxial alignment. Furthermore, as our designs do not require integration of external devices, it enables the construction of a standalone, compact, single-material soft robotic arm.

2. Results and Discussion

As shown in Figure 1a, our multifunctional soft robotic arm consists of three different types of actuators. They provide two

degrees of freedom, namely, in and out of the plane. The rotating base is responsible for the motion in X- and Y-axes. It consists of a nichrome heating element embedded in an LCE pillar with helical alignment, established by rolling a uniaxially aligned LCE film around the nichrome wire and subsequently twisting it by 720°. The actuation of the LCE rotating base can be activated by triggering the Joule effect with current, which is enhanced by the positioning of the heating element within the LCE. The principle of the actuation lies in the anisotropic thermal expansion of the helically aligned LC mesogens. The angle of rotation ($\Delta\theta$) can be defined as a function of current (I_1). On the other hand, the uniaxially aligned LCE lifting unit enables motion in the Z-axis and is operated in the same manner as the rotating base. The maximum lifting height (ΔZ) can also be defined as a function of a separate current (I_2). Nichrome wire, as the passive component, hinders deformation of LCEs. However, it further reinforces the rigidity of the LCE and thus makes the system more robust. Most innovatively, we designed a suction cup-based gripper, whose function is based on the reversible flat-to-conical deformation of a photothermal-responsive LCE film with azimuthal alignment.^[27] The underlying principle is the reversible vacuum generation caused by LCE film deformation. Irradiating the gripper with light triggers LCE deformation and negative pressure generation that attaches the target object to the LCE suction cup. As shown in Figure 1b, the two electrical inputs to the soft robotic arm can be visualized as parallel branches within a

circuit. This allows the actuation amplitude of each element in the soft robotic arm to be defined in terms of the magnitude and activation time of the electric input signal. The trajectory of the gripper can be mapped to the actuation of the rotating base and lifting unit by inverse kinematics. As shown in Figure 1c, the motion of the soft robotic arm can be preprogrammed in terms of two independent input electric signals and an incident light intensity, enabling the system to be run a repetitive motion.

The gripper is the most crucial innovation of our soft robotic arm. Inspired by the branchial sucker of an octopus, as shown in **Figure 2a**, it was developed on the principle of suction-based adhesion. We manufactured the suction cup gripper (**Figure 2b**) by the direct-ink-writing printing procedure. As it involves responsive material, this process is referred to as 4D printing,^[27–30] an important aspect of additive manufacturing. **Figure 2c** shows the schematic representation of the printing process. During extrusion and deposition, shear forces and elongational flow influence the LC polymer chain alignment, establishing a molecular order parallel to the direction of the shear flow. Before printing, the acrylate-terminated main-chain LCE was synthesized through a Michael addition reaction,^[31] using Molecule 1 and Molecule 2 with a molar ratio of

1:0.91 (**Figure 2d**). Commercial visible light dye with broad absorption in the visible light region (**Figure S1**, Supporting Information), Disperse Red 1 (Molecule 3), was selected as the photothermal conversion medium to endow the elastomer with light-responsive properties. Molecule 4 was used to initiate the photopolymerization after printing. The liquid crystal mixture exhibits smectic-to-nematic and nematic-to-isotropic phase transition temperatures at ≈ 40 and 90°C , respectively (**Figure S2**, Supporting Information). To establish a flat-to-conical state transition, we utilize the azimuthal alignment, as schematically illustrated in **Figure 2e** (inset). To achieve this alignment, concentric annular extrusion paths were designed. After dissolving the polyvinyl alcohol (PVA) sacrificial layer, a photothermal-responsive suction cup was obtained (as shown in **Figure 2b**) and then assembled with the LCE lifting unit to complete the soft robotic system. The crossed polarizer microscope (POM) was used to check the alignment of LC mesogens. As shown in **Figure 2e**, under POM, the photothermal-responsive suction cup exhibits the expected fan-shaped pattern. The regions where the molecules are parallel to the crossed polarizers appear black. After rotating the crossed polarizers by 45° , the fan-shaped pattern is also rotated 45° . This confirms the

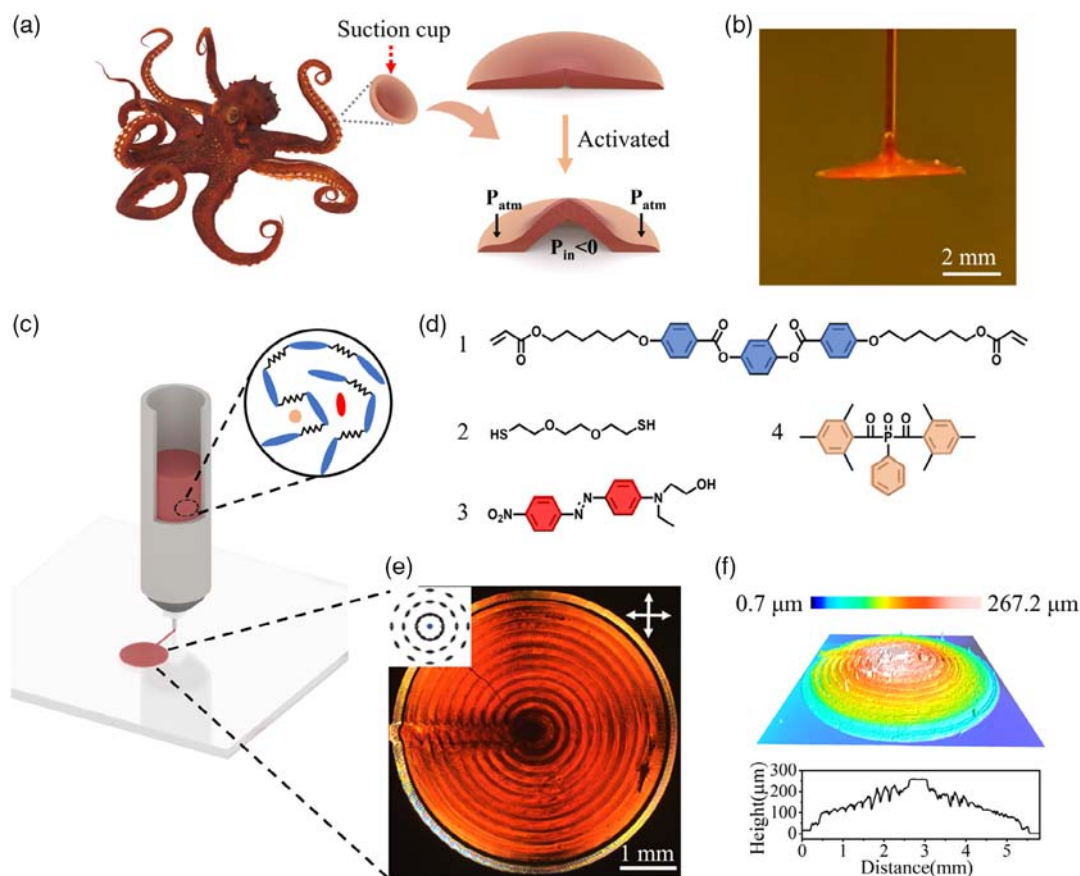


Figure 2. LCE photothermal-responsive suction cup as a gripper. a) Annotated illustrations of an octopus and its branchial limb sucker. P_{atm} represents the atmospheric pressure. b) Photograph of the photothermal-responsive suction cup-based gripper. c) Schematic representation of the printing process. d) Structural formulae of the chemicals used to synthesize the utilized liquid crystal oligomer. e) The initial LCE film observed by optical microscopy between crossed polarizers. The inset schematic depicts the alignment of LC mesogens. f) 3D interferometer image of the photothermal-responsive suction cup surface topography and its corresponding 2D profile along the diameter direction.

azimuthal orientation. We further investigated the surface roughness of the printed LCE suction cup. 3D interferometer results suggest that the initial surface is irregular, as shown in Figure 2f, where small surface reliefs of 10 s of nanometers are observed. Furthermore, the data exhibits a double wedge-shaped profile along the diameter direction. Upon heating, this azimuthally aligned LCE wedge can deform into a cone due to the anisotropic deformation, as shown in Figure 3a. There is no preferred direction in the film with a uniform cross section due to the symmetrical expansion of LC mesogens in the z-axis (Figure S3, Supporting Information).

In order to control this deformation direction, we have engineered the LCE film cross section. As shown in Figure 3b, the film consistently bends upward due to the linearly decreasing film thickness toward the center and along the radial direction. In contrast, as shown in Figure 3c, the film consistently bends downward with a linearly increasing film thickness toward the

center and along the radial direction. The former is the desired configuration for our soft robotic arm.

Upon illumination by an light-emitting diode (LED) lamp (455 nm), the initial flat film deformed into a conical state within 7 s, as shown in Figure 3d and Movie S1, Supporting Information. This is due to the anisotropic expansion of LC mesogens in reaction to the photothermal effect of the visible light dye (Molecule 3). When the LED lamp is switched off, the film relaxes back into its flat state within 6 s. These delays between switching the LED lamp on/off and the complete film actuation have a direct relation with the heating and cooling rates of the film respectively. When the cooling or heating rate increases, the delay decreases. For instance, using a stronger LED light would allow the film to heat up faster and reduce the actuation lag. The viscoelastic nature of the LCE also contributes to activation–actuation mismatch. Beyond kinetics, we further characterized the deformation process by tracking the

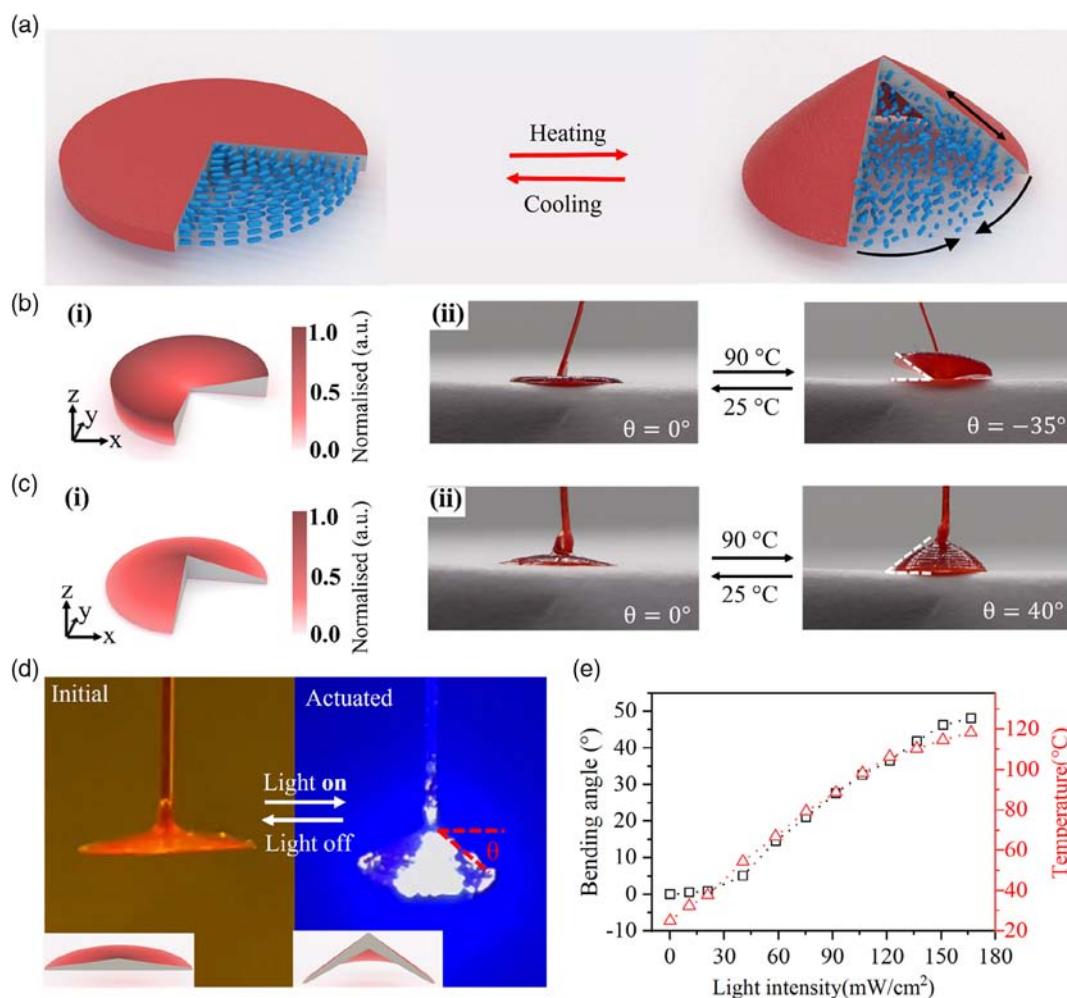


Figure 3. Controlling suction cup-based gripper deformation direction by manipulating film cross section. a) The schematic of actuation behavior in the film with azimuthal alignment. The black arrows show the direction of the LC mesogens contraction. b) The LCE film with a linearly decreasing film thickness toward the center, along the radial direction, leads to upwards deformation. The color bar shows the normalized height. c) The LCE film with a linearly increasing film thickness toward the center, along the radial direction, leads to downward deformation. d) Photothermally triggered actuation behavior of an azimuthal elastomer film upon irradiation by blue light. e) Graphical representation of bending angle and its corresponding temperature against applied light intensity.

position of the printed LCE film when fully actuated under different light intensities. As shown in Figure 3e, increasing the light intensity increases the maximum bending angle θ . Below 40 °C, some deviation between the temperature curve and deformation curve occurred due to the layered structure formed in the smectic phase, which hampers the expansion rate in the direction perpendicular to the director.

After successfully controlling the direction of deformation, we explored the capacity of the actuator as a responsive gripper for pick-and-place operations. As shown in Figure 4a(i–iv), this operation consists of four stages. First, the actuator was placed on the plastic round-topped cylinder (diameter = 6 mm, 335 mg) to ensure complete contact at the interface. Second, the sample

was illuminated with blue light (445 nm) to deform it to its conical state. This formed an enclosed space (Figure 4a(ii)) between the object and the suction cup. Third, illumination by blue light was sustained, increasing LCE deformation and subsequently increasing the bending angle (θ_2) and the volume (V_2) of the enclosed space. This generated an increasing negative pressure (P_2) inside the suction cup. Meanwhile, the atmospheric pressure enhances the attachment of the film to the object, which causes sufficiently high friction to resist slippage. Consequently, as shown in Figure 4a(iii), after applying an upward pulling force, the object is lifted. In the last stage (Figure 4a(iv)), after removing the blue light, the bent membrane spontaneously returns to the initial flat state, reducing the

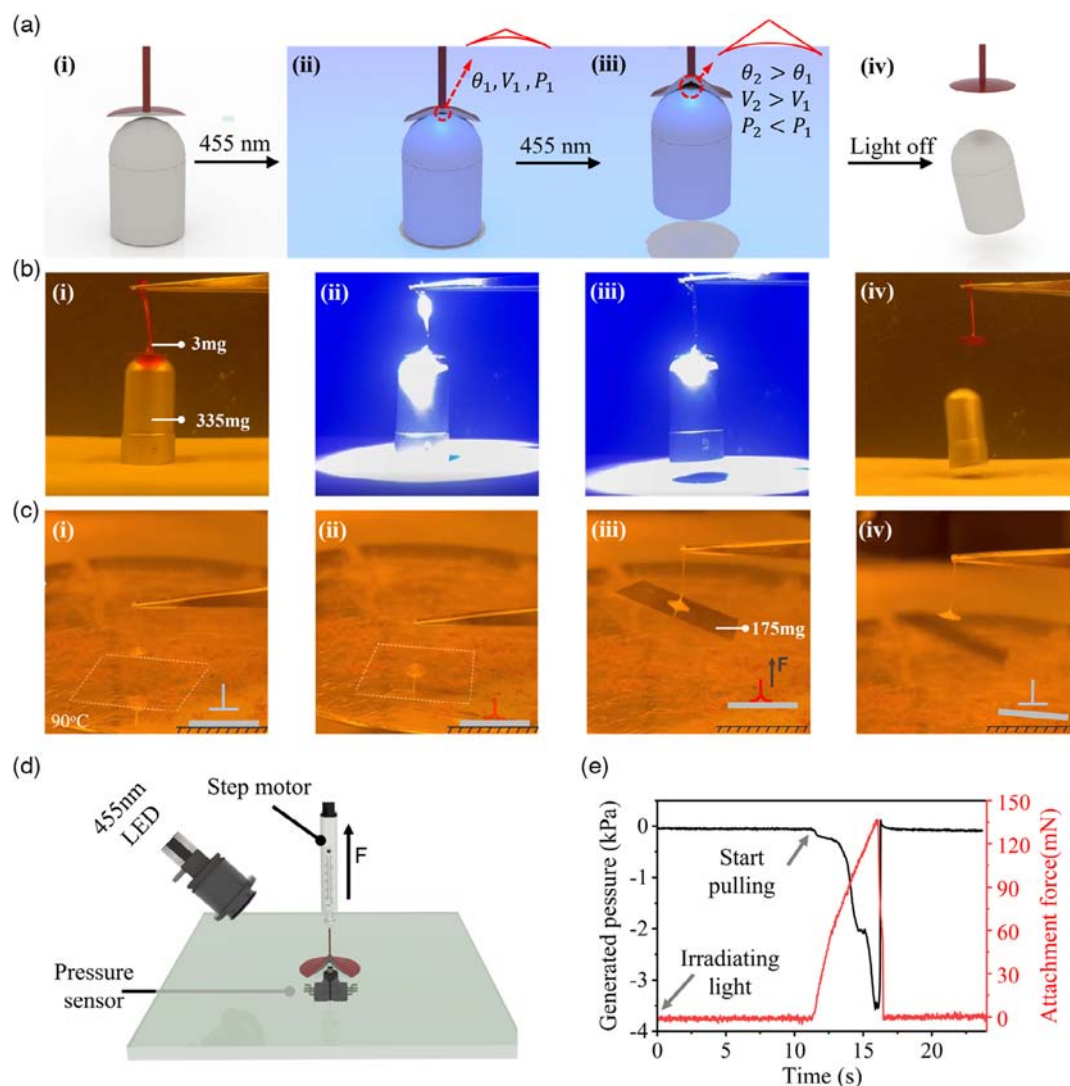


Figure 4. Suction-cup-based gripper for gripping and holding the object. a) The schematics of the gripper engaging an object with surface curvature: initial state i), forming an enclosed space between the suction cup and object ii), generating negative pressure inside the suction cup to grip the object iii), relaxing deformation, and releasing the object iv). The θ , V , and P parameters correspond to the actuated angle, the volume of closed space in the interface, and the air pressure inside the suction cup respectively. b) The pick-and-place procedure of the gripper, which corresponds to the procedure in Figure 4a(i–iv). c) The gripper engaging an object with a flat surface, with insets schematics showing the different states of the LCE gripper. d) The schematic of the home-built setup for measuring attachment force and negative pressure. e) Graphical representation of the attachment force and the pressure difference inside the suction cup with respect to elapsed time while peeling the LCE film off from the glass substrate.

negative pressure inside the LCE cone and releasing the object from the suction cup. The actual pick-and-place procedures of the gripper are shown in Figure 4b, which correspond to the procedure in Figure 4a. To demonstrate its function as a gripper, we apply the LCE suction cup to grip a spherically topped cylinder with smaller curvature of diameter=5 mm (Movie S2, Supporting Information) as well as extremely large curvature (that is flat). The result of grasping the flat substrate is shown on Figure 4c. As this version of the gripper adhering to the flat object contains no azobenzene dye (Molecule 3), the system was thermally activated by heating alone the adhered glass slide to 90 °C on a hotplate prior to contact (Figure 4c(i)). Its grasping process is similar to that achieved through the photothermal suction cup. The solely thermal LCE gripper deformed into its conic state, generating negative pressure inside after contact with the hot glass (Figure 4c(ii)). Upon applying an upward pulling force, the flat glass is lifted successfully. This also causes the gripper to cool rapidly as it is moved away from the hotplate, reducing actuation and subsequently the negative pressure inside. Consequently, the adhered flat glass was released after 8 s.

To further illustrate the potential of the photothermal-responsive suction cup as a gripper, we customized a pressure-sensitive device to quantify the attachment forces in the interface between the LC film and object. The schematic of the custom device is shown in Figure 4d. The photothermal-responsive

suction cup was placed on the substrate with pressure and tension sensors. The photothermal-responsive suction cup was also fixed to a stepper motor, which provided force toward pulling it off the substrate. After irradiating the sample with blue light for 10 s to induce deformation, the photothermal-responsive suction cup was pulled upward at 1 mm s^{-1} , until it was free from the substrate. The pressure and tension sensors were used to monitor the evolution of pressure inside the suction cup and the pulling force in situ. As shown in Figure 4e, during the detachment process, the deformed suction cup can generate up to 3.5 kPa negative pressure. The corresponding attachment force from atmospheric pressure is 39.7 mN. This was calculated considering that the diameter of the actuated suction cup is 3.8 mm. Moreover, the tension sensor measures about 130 mN of force at the detachment event, which suggests that the adhesion forces between the LCE element and the object also contribute to the attachment.

Yet, the suction cup gripper on its own can only achieve a singular function. Therefore, it was attached to a soft robotic arm consisting of multiple LCE actuators to achieve multifactored pick-and-place functions. The schematic and the sample of the assembled robotic arm are shown in Figure 5a,b. In our soft robotic arm, the rotating base was synthesized through the two-step crosslinking process.^[32] The final actuation behavior can be viewed in Figure S5 and Movie S3, Supporting

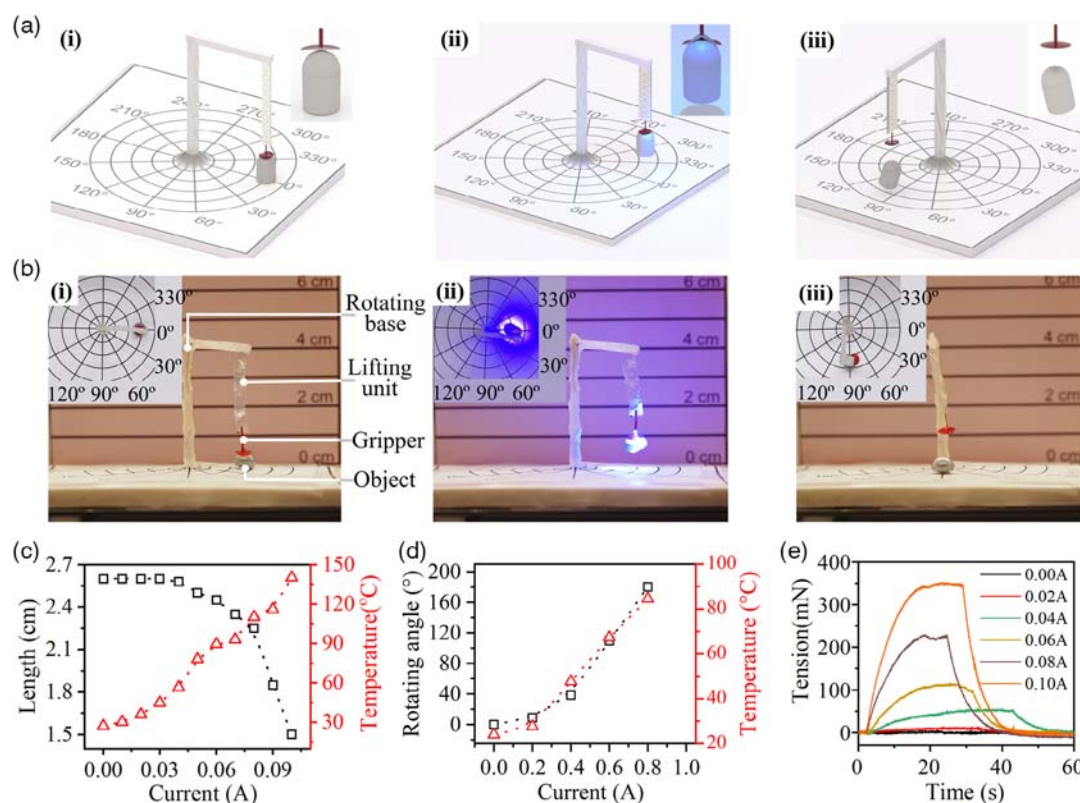


Figure 5. Soft robotic arm for transport and pick-and-place operations in 3D space. a) The schematic of the work procedure of electric signal-driven soft robotic arm: i) initial state, ii) gripping and lifting the object, and iii) finally transporting and releasing the object. The insets show the state of the gripper. b) Photographs of the work procedure of the soft robotic arm, which is corresponding to the schematic in Figure 5a(i-iii). The insets show the corresponding top view in the different states. c) The actuation behavior of the rotating base. d) The actuation behavior of the lifting unit. e) The load capacity of the lifting unit in different applied currents.

Information. As shown in Figure 5c, the final rotation angle is controllable by the input current. The direction of rotation can be selected by changing the twist direction during sample preparation. On the other hand, the lifting unit was fabricated in a similar process to the rotating base, yet the diameter of the embedded nichrome wire was reduced to 50 μm to produce a more compliant heating element. Moreover, the polydomain precured elastomer was stretched instead of twisted. This induces a uniaxial alignment, which is then fixed through photopolymerization. Details on the preparation process and actuation behavior can be viewed in Figures S6 and S7, Supporting Information. Upon current input, actuation is triggered and the lifting unit begins to contract. As shown in Figure 5d, the lifting unit contracted by 52% of its initial length with 0.1 A current input, yet this maximum lifting height can be adjusted by altering the input current. By fixing the length of the lifting unit while heating, we also investigated its actuation tension with different input currents. This experiment was a modified version of the experiment measuring the attachment force of the suction cup. As shown in Figure 5e, the tension can be selected by changing the input current, up to a maximum tension of 350 mN. However, this force is not equivalent to the maximum load capacity of the soft robotic arm, as the attachment force of the suction cup and the flexural stiffness of the rotating base can act as limiting factors.

Next, considering the specific task of the soft robotic arm is to displace an object from the 0° to 90° positions, the operation of the gripper would involve three consecutive stages, as shown in Figure 5ab. Current with different magnitudes can be directed through each element independently, allowing for each element to be activated individually or simultaneously as desired. In the first stage, 0.07 A of current was run through the embedded nichrome wire in the lifting unit, activating material contraction and lifting the held object. In the second stage, 0.55 A of current was applied to actuate rotating base. In the last stage, the circuit running through the rotating base and lifting unit was switched off. This triggers the soft robotic arm to move back to its initial position, ready for the next task. This entire process is recorded in Movie S4, Supporting Information.

In conclusion, we demonstrate the pick-and-place operation capacity of our soft robotic arm. Our LCE photothermal-responsive suction cup gripper is the overarching factor in its function, eliminating the need for any external assistive devices. The LCE photothermal-responsive suction cup was recorded lifting objects 100 times its own weight, yet can theoretically lift objects weighing 40 times more. The attachment force is comparable to a live octopus's sucker under water.^[33] This project highlights the potential of constructing complex soft robots by integrating different types of actuators into one device. Yet, this multifunctional soft robotic arm is constructed from a single material, advertising the prospect of single-material devices. We anticipate that this approach can further improve device mobility, advancing the soft robotics field toward building devices that are applicable in industrial and consumer products and uses.

3. Experimental Section

Materials: An overview of the materials for the photothermal-responsive suction cup is provided in Figure 2d. Molecule 1

(1,4-Bis-[4-(6-acryloyloxyhexyloxy) benzoyloxy]-2-methylbenzene) was purchased from Merck. Molecule 2 (3,6-Dioxo-1,8-octanedithiol), Molecule 3 (N-Ethyl-N-(2-hydroxyethyl)-4-(4-nitrophenylazo) aniline), and basic catalyst (1,8-diazabicyclo[5.4.0]undec-7-ene, DBU) were obtained from Sigma-Aldrich. Molecule 4 (Irgacure 819) was purchased from Ciba. Polyvinyl alcohol with an average molecular weight of 25 000 g mol^{-1} was obtained from Sigma-Aldrich. Dichloromethane was obtained from Biosolve. For fabricating rotating base and lifting unit, pentaerythritol tetrakis(3-mercaptopropionate) (PETMP) and dipropylamine (DPA) were obtained from Sigma-Aldrich.

Synthesis and Processing of the Photothermal-Responsive suction cup: A direct ink writing procedure was used to fabricate an LCE film with azimuthal alignment. First, we synthesized the oligomer via a base-catalyzed thiol-acrylate Michael addition reaction. Molecule 1 (4036.62 mg), Molecule 3 (24.5 mg), and Molecule 4 (49 mg) were added into dichloromethane (3 mL) and the mixture was then heated and stirred at 50 °C to dissolve all solid material. Then, Molecule 2 (875.04 mg) and based catalyst DBU (20 μL) were added to the solution. After stirring for 3 h on a hot plate at 40 °C, the mixture was poured into a poly(tetrafluoroethylene) (PTFE) evaporation dish and then placed in a vacuum oven at 40 °C for 3 h to evaporate the DCM. Second, the oligomer was filled into an ink syringe and then put into a vacuum oven at 80 °C for 20 min to remove any air bubbles. After that, the ink syringe was loaded into the commercial 3D printer (EHR, Hyrel 3D). The oligomer was extruded into a substrate coated with a PVA layer using a nozzle (diameter = 335 μm) at 68 °C. The printing speed was set as 300 mm min^{-1} and the printing path was preprogrammed by G-code generated by the printer software. After printing, an Exfo Omnicure S2000 light source was used to photopolymerize the aligned oligomer at room temperature for 2 h, while the sample was flipped every 30 min. After photopolymerization, the sample was immersed in water at room temperature for 20 min to dissolve the PVA layer. Finally, after further drying the sample at room temperature, a free-standing film with azimuthal alignment was obtained.

Synthesis and Processing of the Rotating Base: The rotating base was manufactured through a two-step crosslinking procedure, following previously reported work^[32] with little modification. The procedure of preparing the rotating base is shown in Figure S4, Supporting Information. First, reactive liquid crystal mesogens RM 257 (1200 mg) and photoinitiator Irgacure 819 (12 mg) were added into dichloromethane (1000 μL), and the mixture was heated and stirred at 50 °C to dissolve all the solids. Then, the solution was placed in a vacuum oven at 70 °C for 3 h to evaporate all the DCM and avoid monomer crystallization. Next, PETMP (91.67 mg), Molecule 2 (273.6 mg) and DPA (3 μL) were immediately added into the solution. After stirring, the solution was poured into the rectangular mold (thickness = 500 μm) and left to dry at room temperature for 24 h. Second, nichrome wire (diameter = 200 μm) was placed on the edge of the precrosslinked film, and then the film was rolled up to form a pillar with a diameter of about 2.5 mm. Finally, after the pillar was twisted 720°, an Exfo Omnicure S2000 light source was used to photopolymerize the aligned oligomer at room temperature for 3 h, while the sample was flipped every 30 min. Thereby, an electric responsive actuator for rotating was obtained.

Synthesis and Processing of the Lifting Unit: The lifting unit was fabricated in a similar procedure to the rotating base. The procedure of preparing the lifting unit is shown in Figure S6, Supporting Information. Differences include thinner nichrome wire (diameter = 50 μm) being embedded in the precured oligomer to get a more flexible actuator. Then, the precured oligomer was stretched to get uniaxial alignment. Finally, photopolymerization was used to fix the uniaxial alignment.

Characterization Methods: Differential scanning calorimetry (DSC) measurements were employed to determine the transition temperature of oligomers in TA Instruments DSC Q1000. The POM images of the suction cup were taken from a Leica DM 2700M equipped with two polarizers. The thickness and surface topography was determined via the 3D Optical Profiler (Sensofar Metrology). The photothermal-responsive suction cup was actuated by collimated visible light (455 nm, Thorlabs M455L2), in which a controller (Thorlabs DC4104) was used to tune the intensity

of the lights. The rotating base and lifting unit were actuated by a DC power source (TENMA 72-2720).

Supporting Information

Supporting Information is available from the Wiley Online Library or from the author.

Acknowledgements

The authors thank Professor Dirk J. Broer for his support and guidance for this project. The authors also thank Dr. Thierry K. Slot for helping build the electronic setup used to measure negative pressures within the liquid crystal elastomer suction cup. The authors also thank financial support from CRT Starterspakket from ICMS, Eindhoven University of Technology, the Netherlands Organization for Scientific Research (NWO OCENW.KLEIN.10854, START-UP 8872), the European Union's Horizon 2020 Research and Innovation Programmer under the Marie Skłodowska-Curie grant agreement no. 956150 (STORM-BOTS). C.S.S. thanks the Spanish "Ministerio de Ciencia, Innovación y Universidades (MCIU)" through AEI/FEDER(UE) project PID2020-118485RB-I00.

Conflict of Interest

The authors declare no conflict of interest.

Data Availability Statement

The data that support the findings of this study are available from the corresponding author upon reasonable request.

Keywords

electrically driven, liquid crystal elastomers, multifunctional single materials, pick-and-place operations, soft robotic arms

Received: August 23, 2022

Revised: September 28, 2022

Published online: November 26, 2022

- [1] M. A. K. Bahrin, M. F. Othman, N. H. N. Azli, M. F. Talib, *J. Teknol.* **2016**, *78*, 6.
- [2] B. Preising, T. C. Hsia, B. Mittelstadt, *IEEE Eng. Med. Biol. Mag.* **1991**, *10*, 13.
- [3] H. Cruse, *Biol. Cybern.* **1986**, *54*, 125.
- [4] K. Suzumori, S. Iikura, H. Tanaka, *IEEE Control Syst. Mag.* **1992**, *12*, 21.

- [5] N. Vasios, A. J. Gross, S. Soifer, J. T. B. Overvelde, K. Bertoldi, *Soft Robot.* **2020**, *7*, 1.
- [6] F. Ilievski, A. D. Mazzeo, R. F. Shepherd, X. Chen, G. M. Whitesides, *Angew. Chem. Int. Ed.* **2011**, *50*, 1890.
- [7] R. Deimel, O. Brock, *Int. J. Rob. Res.* **2016**, *35*, 161.
- [8] H. Jiang, Z. Wang, Y. Jin, X. Chen, P. Li, Y. Gan, S. Lin, X. Chen, *Int. J. Rob. Res.* **2021**, *40*, 411.
- [9] G. Oliveri, L. C. van Laake, C. Carissimo, C. Miette, J. T. B. Overvelde, *Proc. Natl. Acad. Sci.* **2021**, *118*, 2017015118.
- [10] S. Li, D. M. Vogt, D. Rus, R. J. Wood, *Proc. Natl. Acad. Sci. USA* **2017**, *114*, 13132.
- [11] B. Gorissen, E. Milana, A. Baeyens, E. Broeders, J. Christiaens, K. Collin, D. Reynaerts, M. De Volder, *Adv. Mater.* **2019**, *31*, 1804598.
- [12] H. Wermter, H. Finkelmann, *E-polymers* **2001**, *1*, 111.
- [13] B. Jin, J. Liu, Y. Shi, G. Chen, Q. Zhao, S. Yang, *Adv. Mater.* **2022**, *34*, 2107855.
- [14] Y. Yu, M. Nakano, T. Ikeda, *Nature* **2003**, *425*, 145.
- [15] S. Ma, X. Li, S. Huang, J. Hu, H. Yu, *Angew. Chem. Int. Ed.* **2019**, *58*, 2655.
- [16] Y. Zhang, Z. Wang, Y. Yang, Q. Chen, X. Qian, Y. Wu, H. Liang, Y. Xu, Y. Wei, Y. Ji, *Sci. Adv.* **2020**, *6*, eaay8606.
- [17] X. Lu, S. Guo, X. Tong, H. Xia, Y. Zhao, *Adv. Mater.* **2017**, *29*.
- [18] H. Zeng, O. M. Wani, P. Wasylczyk, R. Kaczmarek, A. Priimagi, *Adv. Mater.* **2017**, *29*, 1701814.
- [19] J. Sun, Y. Wang, W. Liao, Z. Yang, *Small* **2021**, *17*, 1.
- [20] M. Barnes, R. Verduzco, *Soft Matter* **2019**, *15*, 870.
- [21] C. Zhu, Y. Lu, L. Jiang, Y. Yu, *Adv. Funct. Mater.* **2021**, *31*, 1.
- [22] Z. Cheng, T. Wang, X. Li, Y. Zhang, H. Yu, *ACS Appl. Mater. Interfaces* **2015**, *7*, 27494.
- [23] X. Lu, H. Zhang, G. Fei, B. Yu, X. Tong, H. Xia, Y. Zhao, *Adv. Mater.* **2018**, *30*, 1706597.
- [24] B. Zuo, M. Wang, B.-P. Lin, H. Yang, *Nat. Commun.* **2019**, *10*, 4539.
- [25] D. Liu, C. W. M. M. Bastiaansen, J. M. J. J. Den Toonder, D. J. Broer, *Macromolecules* **2012**, *45*, 8005.
- [26] P. Lv, Y. You, J. Li, Y. Zhang, D. J. Broer, J. Chen, G. Zhou, W. Zhao, D. Liu, *Adv. Sci.* **2004749**.
- [27] M. López-Valdeolivas, D. Liu, D. J. Broer, C. Sánchez-Somolinos, *Macromol. Rapid Commun.* **2017**, *39*, 1700710.
- [28] T. H. Ware, Z. P. Perry, C. M. Middleton, S. T. Iacono, T. J. White, *ACS Macro Lett.* **2015**, *4*, 942.
- [29] M. Barnes, S. M. Sajadi, S. Parekh, M. M. Rahman, P. M. Ajayan, R. Verduzco, *ACS Appl. Mater. Interfaces* **2020**, *12*, 28692.
- [30] M. Fang, T. Liu, Y. Xu, B. Jin, N. Zheng, Y. Zhang, Q. Zhao, Z. Jia, T. Xie, *Adv. Mater.* **2021**, *33*, 2105597.
- [31] T. H. Ware, M. E. McConney, J. J. Wie, S. K. Ahn, V. P. Tondiglia, T. J. White, *Science* **2015**, *347*, 982.
- [32] Y. Wang, J. Sun, W. Liao, Z. Yang, *Adv. Mater.* **2022**, *34*, 2107840.
- [33] H. Bagheri, A. Hu, S. Cummings, C. Roy, R. Casleton, A. Wan, N. Erjavic, S. Berman, M. M. Peet, D. M. Aukes, X. He, S. C. Pratt, R. E. Fisher, H. Marvi, *Adv. Intell. Syst.* **2020**, *2*, 1900154.